International Journal of Bioprinting

RESEARCH ARTICLE

Integrating zinc/silicon dual ions with 3D-printed GelMA hydrogel promotes *in situ* hair follicle regeneration

Fanliang Zhang[1†], Zhaowenbin Zhang[2†], Xianlan Duan[1], Wei Song[1], Zhao Li[1], Bin Yao[1], Yi Kong[1], Xing Huang[3], Xiaobing Fu[1], Jiang Chang[2,4*], Sha Huang[1*]

[1]Research Center for Tissue Repair and Regeneration Affiliated to the Medical Innovation Research Department, PLA General Hospital, Beijing, 100853, China

[2]Wenzhou Institute, University of Chinese Academy of Sciences, Wenzhou, Zhejiang 325000, China

[3]Key Laboratory of Photochemical Conversion and Optoelectronic Materials, Technical Institute of Physics and Chemistry, Chinese Academy of Sciences, Beijing, 100190, China

[4]State Key Laboratory of High Performance Ceramics and Superfine Microstructure, Shanghai Institute of Ceramics, Chinese Academy of Sciences, Shanghai, 200050, China

(This article belongs to the *Special Issue: Integrated Biofabrication Technologies for Constructing Functional Tissue*)

Abstract

The regeneration of hair follicles lost from injury or disease represents a major challenge in cutaneous regenerative medicine. In this study, we investigated the synergetic effects between zinc and silicon ions on dermal cells and screened the optimal concentration of ions for medical applications. We integrated zinc/silicon dual ions into gelatin methacryloyl (GelMA) to bioprint a scaffold and determined that its mechanical properties are suitable for biological treatment. Then, the scaffold was employed to treat mouse excisional model in order to promote *in situ* hair follicle regeneration. Our findings showed that GelMA-zinc/silicon-printed hydrogel can significantly activate hair follicle stem cells and enhance neovascularization. The beneficial effects of the scaffold were further confirmed by the growth of hairs in the center of wounds and the improvement in perfusion recovery. Taken together, the present study is the first to combine GelMA with zinc/silicon dual ions to bioprint *in situ* for treating excisional wound, and this approach may regulate hair follicle regeneration not only directly by impacting stem cells but also indirectly through promoting angiogenesis.

Keywords: Zinc and silicon ions; 3D bioprinting; GelMA; Hair follicle regeneration; Angiogenesis

†These authors contributed equally to this work.

***Corresponding authors:**
Sha Huang
(stellarahuang@sina.com)

Jiang Chang
(jchang@mail.sic.ac.cn)

Citation: Zhang F, Zhang Z, Duan X, *et al*., 2023, Integrating zinc/silicon dual ions with 3D-printed GelMA hydrogel promotes in situ hair follicle regeneration. *Int J Bioprint,* 9(3): 703. https://doi.org/10.18063/ijb.703

Received: November 25, 2022
Accepted: January 13, 2023
Published Online: March 8, 2023

1. Introduction

After dermal injury, adult skin wound typically heals with the formation of scar tissue and appendages, including hair follicles, which will be lost and cannot be completely recreated[1-3]. However, in some situations, mouse dorsal skin is capable of regenerating functional hair follicles, which is described as the neogenic hair follicles growing from the center of the wound to its margin[4]. The manner of regeneration is called *in situ* hair

follicle regeneration whose mechanisms are considered the same as the development process during the embryonic period[5]. Determining and utilizing the mechanisms of *in situ* regeneration may contribute to novel approaches to scar-free wound healing and alopecia.

Recently, bioactive ions have been extensively investigated in the areas of regenerative medicine and tissue engineering. For therapeutic applications, bioactive ions have some advantages, such as being inexpensive, easily accessible, chemically stable, and potentially safer than products of genetic engineering[6,7]. Accumulating evidence has shown that bioactive ions have beneficial effects on regulating specific cell behaviors. Zinc (Zn) is an essential trace element of hair follicles and can induce differentiation of adipocytes, suggesting that Zn may function as a stimulus in promoting hair follicles growth in the future[8]. Silicon (Si) ion has stimulatory effects on angiogenesis, and some bioactive materials based on silicate can regulate cell–cell interactions and hair follicle stem cells (HFSCs) activities to accelerate wound healing[9,10]. The biological effects of the two ions imply that they may be valuable for wound repair.

Based on the extensive effects of Zn and Si ions in regenerative medicine, we hypothesized that the interactions between HFSCs and endothelial cells may be regulated by the two ions, which promote *in situ* hair follicle regeneration and angiogenesis in the excisional wound. To confirm our hypotheses, we first investigated the effects of Si and Zn ions on migration and proliferation of different cells as well as blood vessel formation to determine a suitable concentration of ion solution.

However, bioactive ions such as Si or Zn ions have several limitations, such as the difficulty of being fabricated into three-dimensional (3D) scaffolds and a rapidly scattered site which scarcely matches the demand of *in situ* regeneration. Integrating multiple biocompatible factors into 3D-printed hydrogel-based scaffolds is a practical and effective approach to improving skin repair efficacy[11,12]. Gelatin methacryloyl (GelMA) is one of the widely used natural bioinks for 3D-printed hydrogel-based scaffolds due to their excellent features of biocompatibility and degradability, as well as desirable release profiles[13]. In this study, we integrated the solution containing identified bioactive concentration of ions with 3D-printed GelMA hydrogel and then treated excisional wound in mice to observe the synergetic effects on wound healing, perfusion recovery and *in situ* regeneration of hair follicle.

2. Materials and methods

2.1. Materials

We obtained two ion solutions from Chinese Academy of Sciences: one only contains Si ions (120 μg/mL), and the other contains Zn/Si dual ions (Si 120 μg/mL and Zn 20 μg/mL). GelMA and photoinitiators were obtained from EFL (Jiangsu, China). Hydrocolloid wound dressing was purchased from Roosin (Jiangsu, China).

2.2. Studying the effects of ions on cells migration

To determine the optimal concentration of ions, we prepared a series of gradient concentration of solutions (1/64, 1/32, 1/16, 1/8) diluted with corresponding media (DMEM, SH30243.01, Hyclone, USA; HUVEC specific medium, iCell-h110-001b, iCell, China). Then, scratch wound healing assay was employed to assess the migration of human skin fibroblasts (HSFs), human umbilical vein endothelial cells (HUVECs), human immortalized keratinocytes (HaCaTs), and hair follicle dermal papilla (DP) cells in media with different concentration of ions[14]. Briefly, cells were seeded in six-well plates and cultured up to about 80% confluent. Then, a plastic tip (200 μL) was used to scrap the cell monolayer in each well, and the original media was replaced with serum-free media containing ions. At 0, 12, and 24 h, an optical microscope (Leica DMI 4000 B, Germany) was used to capture optical images. ImageJ was employed to analyze the migration rate, which was calculated as the percentage of the remaining area (A) to the initial wound area (A_0).

$$\text{Cell migration rate} = \frac{A_0 - A}{A_0} \times 100\% \quad \text{(I)}$$

where A is the wound area value of all groups at each time-point, and A_0 is the wound area value of the corresponding group at 0 h.

2.3. Studying the beneficial effects of ions on cell viability

Then, the viability of different cells was evaluated by a Cell Counting Kit (CCK-8) assay (CK04, Dojindo, Japan) after treatment with different concentration of ions. HSFs, HUVECs, HaCaTs, and DP cells were respectively seeded into 96-well plates at 3×10^3 cells per well and cultured in the corresponding complete media for 24 h. Then, the original media was replaced by 100 μL ions solutions diluted by complete media. Then, the cells were continuously cultured for 4 days, and a CCK-8 assay was applied to cells at 1st, 2nd, 3rd and 4th day. A multimode microplate reader (Tecan Spark 10M, Switzerland) was employed to measure the absorbance of the reaction product at a wavelength of 450 nm. The results were calculated according to Equation II:

$$\text{Cell viability rate} = \frac{OD_e - OD_b}{OD_b} \quad \text{(II)}$$

The optical density (*OD*) in experimental groups (Si, Zn/Si) was designated as OD_e, and that in control group was OD_b.

2.4. Tube formation assay

The effects of ions on angiogenesis were evaluated by tube formation assay. Briefly, Matrigel (356234, Corning, USA) was added into 48-well plates and was solidified. Then, HUVECs (2×10^4 per well) were seeded into the wells and treated with ions in different concentrations. After incubation for 8 h, an inverted optical microscope (Leica DMI 4000 B, Germany) was employed to capture the images, and the length of the tube and the number of branch points were counted by ImageJ[15].

2.5. Preparation of hydrogels integrated with silicon/zinc ions

Briefly, 1 g of GelMA was dissolved in 5 mL phosphate-buffered saline (PBS) containing lithium phenyl (2,4,6-trimethylbenzoyl) photoinitiator (EFL-LAP, EFL, China) and then, the solution was put into a water bath at 37°C for 1 h. About 312.5 μL Zn/Si dual ions solution was added to 5 mL GelMA hydrogel solution and then, PBS was added to 10 mL, which means the final concentration of ions reached the level of 1/32 Zn/Si ions solution (Zn 0.625 μg/mL, Si 3.75 μg/mL). The hydrogel with Zn/Si dual ions was named GelMA-Zn/Si, and the hydrogel without ions was named GelMA for control.

2.6. Structural characterization

A scanning electron microscope (SEM; S-4800, Hitachi, Japan) was employed to characterize the structure of hydrogels[16]. Briefly, the hydrogels were dehydrated by freeze-drying and were coated with gold-palladium in a Hitachi ion sputter. Then, the images were captured, and the pore size and the porosity were quantified via ImageJ.

$$\text{Porosity} = \frac{\text{Pore area}}{\text{Total area}} \times 100\% \quad \text{(III)}$$

2.7. Swelling property

Samples were shaped into cylinders (height = 10 mm and diameter = 20 mm) whose values of initial weight were recorded as W_0. Then, the hydrogels were put into PBS solution (pH = 7.4) for complete swelling at 37°C, and the values of constant mass were recorded as W_t. The swelling ratio was calculated according to Equation IV[17].

$$\text{Swelling ratio} = \frac{W_t - W_0}{W_0} \quad \text{(IV)}$$

2.8. Rheological test

A rheometer (TA-ARES G2, USA) with a 40 mm-diameter parallel plate was applied to assess the rheological properties of the hydrogels. Frequency sweep tests were conducted from 0.1 to 100 rad/s at 1% strain amplitude at 25°C. The elastic modulus (G′) and viscous modulus (G′) were investigated as a function of frequency[18].

2.9. Compression test

A universal testing machine (Instron 3365, UK) with a 100-N load was employed to perform the compression tests. Samples were shaped into cylinders (height = 10 mm and diameter = 20 mm) and were compressed at a strain velocity of 1 mm/min until fracture at 25°C. The displacement in the hydrogel height and the increasing load were recorded. Then, typical curves were obtained and the first 15%–25% of the curve was used to calculate Young's modulus[17].

2.10. *In vitro* degradation

The initial dry weight of the hydrogels was recorded (W_0). Then, the samples were shaped into cylinders (height = 10 mm and diameter = 20 mm) and were incubated in PBS at 37°C. The PBS was replaced by the fresh solution at determined time intervals, and the dry weight of the remaining hydrogels was recorded (W_d) at different time points. The degeneration rate was calculated according to Equation V[19].

$$\text{Remaining mass of the hydrogel} = \frac{W_d}{W_0} \times 100\% \quad \text{(V)}$$

2.11. Releasing profile of ions from hydrogel

1 mL solidified GelMA-Zn/Si hydrogel was immersed in PBS (pH = 7.4, 9 mL) at 37°C. At predetermined time points (1, 3, 5, and 7 days), samples were collected, and the concentration of ions was measured by inductively coupled plasma emission spectrometer (ICP).

2.12. Mouse excisional model and hydrogel treatment

Female C57 mice aged 4 weeks were obtained from SPF Biotechnology Company (China). GelMA were adequately exposed to ultraviolet light for sterilization, and Zn/Si dual ions solution was sterilized through 0.22-micrometer-pore-size filters (SLGVR33RB, Millipore, Germany). The PBS was sterilized at 124°C for 30 min, and then, the sterile GelMA-Zn/Si hydrogel was prepared. The mouse excisional wound model was established after being anaesthetized with pentobarbital sodium solution (100 mg/kg)[20]. A wound with a diameter of 10 mm was created. Then, the GelMA-Zn/Si hydrogel was loaded into a syringe. One milliliter hydrogel was *in situ* printed and fully covered the wounds. White light was employed to crosslink the hydrogel for 60 s. Gauze and bandage were employed to dress the wound surface. A new hydrogel dressing was replaced every 3 days. In addition, we set another three groups using saline, hydrocolloid and pure GelMA, respectively, for comparison with GelMA-Zn/Si group. Gross images of the wound area were captured on days 0, 7, and 14 postoperation, and 1-cm diameter rubber rings were used as a size reference.

2.13. Histological analysis

Fourteen days after the treatment, all the mice were euthanized to harvest wound skin for histological examination. After being fixed in 4% paraformaldehyde for 6 h, the samples were embedded in O.C.T. Compound (Optimal Cutting Temperature, Sakura, Japan) and were cut into 7-μm sections[21]. Then, hematoxylin (G1150, Solarbio, China) and eosin (G1100, Solarbio, China) (H&E) were employed to stain the sections. Observations were performed with a microscope (Olympus DP72, Japan).

For immunostaining, antigen retrieval and blocking were performed, and sections were incubated for 18 h at 4°C with primary antibodies (CK19 [1:300, ab76539, Abcam, USA], CD31 [1:300, ab24590, Abcam, USA], α-SMA [1:500, ab32575, Abcam, USA]). Then, sections were incubated with CoraLite488-conjugated Goat Anti-Rabbit IgG (1:300, SA00013-2, Proteintech, USA) and CoraLite594-conjugated Goat Anti-Mouse IgG (1:300, SA00013-3, Proteintech, USA) for 2 h in the dark at room temperature. Finally, 4′,6-diamidino-2-phenylindole (DAPI) Fluoromount-G (0100-20, SouthernBiotech, USA) was added to the sections, and pictures were captured with a confocal microscope (Olympus TCS SP8, Japan)[21]. Then, pictures were applied for the analysis of HFSCs activation and angiogenesis. The number of HFSCs was quantified according to the CK 19 staining. The intensity of CD31 and α-SMA double staining was measured by ImageJ.

2.14. Hair follicle differentiation-related gene expression

To evaluate the influences of GelMA-Zn/Si hydrogel on expression of genes related to angiogenesis and hair follicle regeneration, on the 14th day, the wound skin was harvested to extract RNA, using TRIzol reagent (15596018, Invitrogen, USA), for quantitative reverse-transcription polymerase chain reaction (qRT-PCR). A NanoPhotometer (Impen P-Class, Germany) was employed to assay the concentrations of total RNA. Then, a Prime-Script RT reagent kit (RR047Q, Takara Bio, Japan) was applied to synthesize cDNA. Primers for hair neogenesis and angiogenesis containing *Vegf* (vascular endothelial-derived growth factor), *Egf* (epidermal growth factor), *Igf1* (insulin-like growth factor 1), *Kgf* (keratinocyte growth factor), *Pdgfa* (platelet-derived growth factor subunit a), *Pdgfb* (platelet-derived growth factor subunit b) and the housekeeping gene, *Gapdh*, were synthesized by Tsingke Biotechnology (China)[22,23]. Quantitative analysis of gene expression was performed on a QuantStudio 5 system (Thermo Fisher Scientific, USA). The gene expression level was normalized to that of *Gapdh*, and the data was analyzed by the $2^{-\Delta\Delta Ct}$ method. The sequences of primers are given in Table 1.

Table 1. Primer sequences

Gene (forward or reverse)	Sequence (5′–3′ direction)
Vegf (F)	5′-GCACATAGAGAGAATGAGCTTCC-3′
Vegf (R)	5′-CTCCGCTCTGAACAAGGCT-3′
Igf1 (F)	5′-AAATCAGCAGCCTTCCAACTC-3′
Igf1 (R)	5′-GCACTTCCTCTACTTGTGTTCTT-3′
Egf (F)	5′-CGAATGGTGCAGTAGTAGATGC-3′
Egf (R)	5′-GTCTCCATGAAGTCAGATGCAC-3′
Kgf (F)	5′-CTCTACAGGTCATGCTTCCACC-3′
Kgf (R)	5′-ACAGAACAGTCTTCTCACCCT-3′
Pdgfa (F)	5′-GGACCTGGGCTTGCCTGCTGCTC-3′
Pdgfa (R)	5′-GGGCGGCCGGCTCTATCTCACC-3′
Pdgfb (F)	5′-AAGTGTGAGACAATAGTGACCCC-3′
Pdgfb (R)	5′-CATGGGTGTGCTTAAACTTTCG-3′
Gapdh (F)	5′-AACGACCCCTTCATTGACCT-3′
Gapdh (R)	5′-ATGTTAGTGGGGTCTCGCTC-3′

2.15. Blood perfusion evaluation

Mice were anaesthetized with 1% pentobarbital sodium solution and fixed on a heated platform in a supine position. A PeriCam PSI-ZR (Sweden) was employed to measure perfusion value of each wound. PIMSoft (Moor Instruments Ltd, UK) was used to analyze the mean perfusion volume of each wound[24].

2.16. Statistical analysis

The data are expressed as means ± standard deviation and were processed using the statistical software GraphPad Prism 8.0. A *t*-test was used for comparison between two groups at the same time-point. One-way analysis of variance (ANOVA) was performed to compare the differences between multiple groups at the same time-point. Two-way ANOVA was performed to compare the differences between multiple groups at different time-points. Statistical significance was considered when $^{*}P < 0.05$, $^{**}P < 0.01$, $^{***}P < 0.001$, $^{****}P < 0.001$.

3. Results

3.1. Synergistic effects of Zn ions and Si ions on the migration of cells

In the study, we employed two ion solutions. To investigate the synergistic effects of ions on cell proliferation and screen the optimal ions concentration for the following animal experiments, we prepared a series of concentration gradient of solutions. Next, we evaluated the impact of ions on cell migration. As shown in Figure 1A and B, after co-incubation for 12 and 24 h, all the HSFs groups treated with ion solutions migrated significantly faster than the control group. The average migration ratio of 1/32 Zn/Si solution

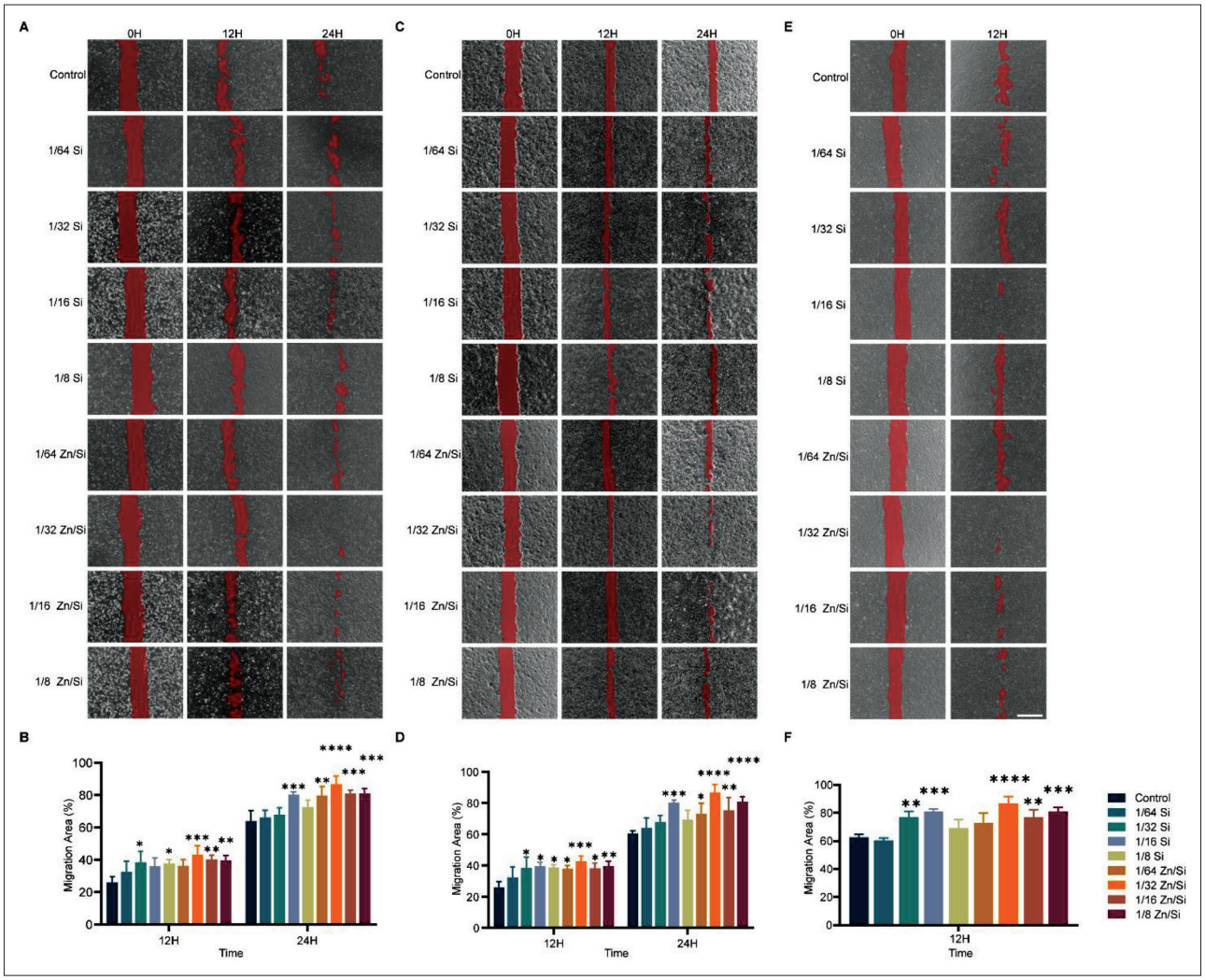

Figure 1. Synergistic effect of various concentration of ions on migration of different cells. (A) Typical images of HSFs treated with various concentration of ions. (B) Quantitative analysis of scratch wound areas. (C) Typical images of HaCaTs treated with various concentration of ions. (D) Quantification of scratch wound areas. (E) Typical images of HUVECs treated with ions. (F) Quantitative analysis of scratch wound areas. *$P < 0.05$, **$P < 0.01$, ***$P < 0.001$, ****$P < 0.0001$. N = 3 for each time point. All the analyses were performed with two-way ANOVA. Scale bar = 500 μm.

(86.77 ± 5.01%) is the highest among the groups and is significantly higher than the control group (63.94 ± 6.56%). These results revealed that Zn ions with Si ions possess great biocompatibility and can facilitate cell migration further, accelerating wound healing. Intriguingly, at 24 h after treatment, there were four groups with significant differences in Zn/Si solution, while only one group in Si solution, which means the combination of Zn and Si ions is more efficient than pure Si ions. Wound healing and hair follicle regeneration are influenced not only by fibroblasts but also by keratinocytes and endothelial cells[25-27]. Therefore, we performed the scratch wound healing assay with HaCaTs and HUVECs to investigate the synergistic effects of ions on the cells. At 24 h after treatment, all HaCaTs groups with Zn/Si ions significantly increased in migration area, while only one group with pure Si ions had a statistical difference compared to the control group (Figure 1C and D). The 1/32 Zn/Si group had the highest mean value. In the case of HUVECs, there was a similar tendency that the 1/32 Zn/Si group possesses the strongest effect on cell migration (Figure 1E and F). To determine the effect of ions on hair follicle *in vitro*, we employed dermal papilla (DP) cells to perform migration assay. After co-incubation for 12 h, all the groups had no significant difference in migration area (**Figure S1A** and **B**). However, at 24 h after treatment, 1/16 Si group and all Zn/Si groups had larger migration area than the control group, which indicates that Zn and Si ions have synergetic effect and can promote DP cell migration. The mean value of the 1/32 Zn/Si group is the biggest among the groups, which

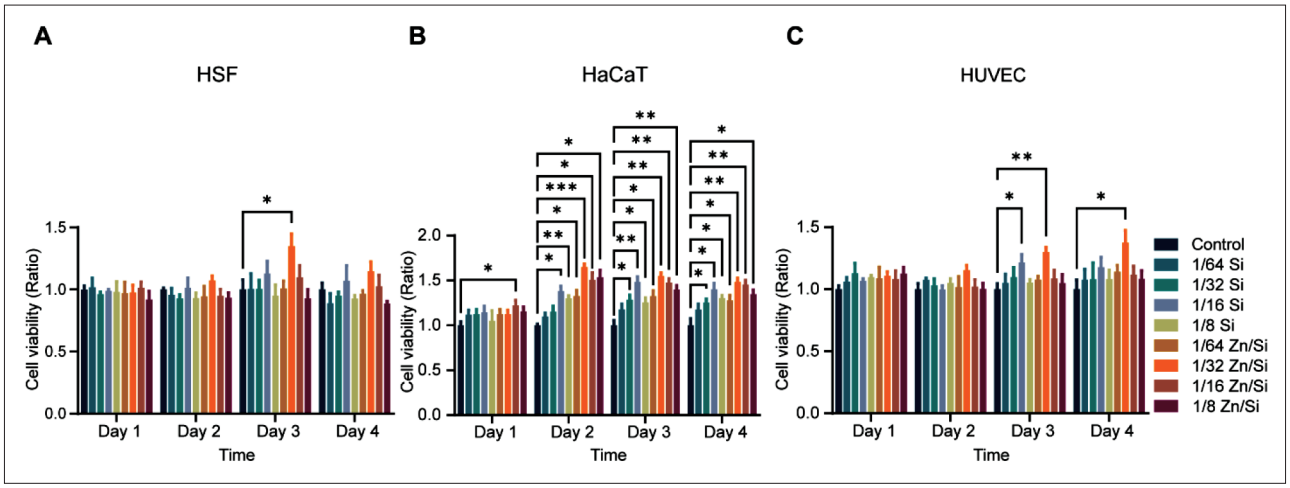

Figure 2. Cell viability of cells cultured with different concentration of ions. (A) Percent of the viability of HSFs co-cultured with different concentrations of ions. (B) Percent of the viability of HaCaTs co-cultured with different concentrations of ions. (C) Percent of the viability of HUVECs co-cultured with different concentrations of ions. *$P < 0.05$, **$P < 0.01$, ***$P < 0.001$. N = 3 for each time point. All the analyses were performed with two-way ANOVA.

suggests that the concentration may be optimal for DP cells. Therefore, Zn/Si at 1/32 dilution ratio (Zn 0.625 μg/mL, Si 3.75 μg/mL) may be the optimal concentration for the following experiments.

3.2. Synergistic effects of Zn ions and Si ions on the viability of cells *in vitro*

To further confirm the optimal concentration of ions, we determined the effects of ions on the viability of cells through CCK-8 assays, and the results are shown in Figure 2. At various dilution ratios from 1/64 to 1/8, two ion solutions showed no cytotoxicity against HSFs. Zn/Si solution at 1/32 dilution ratio revealed a stimulatory effect on HSFs proliferation on the 3rd day after treatment. Although the data of the groups on the 4th day have no significant difference, there still is a tendency that 1/32 Zn/Si solution can promote HSFs proliferation (Figure 2A). In addition, we investigated the effect of pure Zn ion solution (20 μg/mL) on HSFs by CCK-8 assay, and there was no obvious difference among the groups, indicating that Zn ion solution alone cannot significantly accelerate the proliferation of HSFs (**Figure S2**). At dilution ratios of 1/64 to 1/8, two ion solutions maintained the viability of HaCaTs, indicating that these concentrations have no cytotoxic effect against HaCaTs (Figure 2B). All the groups treated with Zn/Si solution had a higher proliferation rate compared to the control group. In Si groups, only 1/16 and 1/8 ratios always had a beneficial effect on HaCaTs, indicating that there may exist a synergistic effect between Zn and Si ions. Similarly, 1/32 Zn/Si solution accelerated the growth of HUVECs on the 3rd and 4th day after intervention (Figure 2C). The effect of ions on DP cells was determined, and the results indicated that 1/32 Zn/Si solution can promote the proliferation of DP cells (**Figure S1C**). These results suggest that Si and Zn ions play a key role in regulating cell proliferation, and the combination of the two ions is more efficient in this regard. About 1/32 Zn/Si solution may be optimal for the following experiments.

3.3. Effect of ions on angiogenesis

Blood vessels can transport nutrition and oxygen for cells around wounds, which have been considered critical for tissue regeneration[28]. There are interactions between endothelial cells and HFSCs during hair follicle regeneration[27]. Therefore, it is essential to identify a proper concentration of ions to promote angiogenesis (Figure 3A). Both ion solutions with appropriate concentration could increase the branch points (Figure 3B) and total length of the tube (Figure 3C), and the 1/32 Zn/Si group had the highest mean value among the groups. Therefore, it can be concluded that the ions promote angiogenesis, and the 1/32 Zn/Si solution may be optimal for the following applications.

3.4. Characterization of hydrogels

After determining the suitable ion concentration for treatment, we added ions to GelMA and then investigated whether ions would affect its physicochemical properties. First, the SEM images display that ions do not change the cross-sectional microstructure of the GelMA hydrogel. Both GelMA and GelMA-Zn/Si hydrogel possess relatively smooth surfaces and interconnecting porous structures and have no difference in internal pore size and porosity (Figure 4A–C, **Figure S3**). Both types of hydrogels exhibited applicable swelling ratios, suggesting that they can absorb tissue exudates and maintain wound moist (Figure 4D)[19]. As for degradation *in vitro*, GelMA-Zn/Si hydrogel still had a faster degradation rate (Figure 4E). As compared with

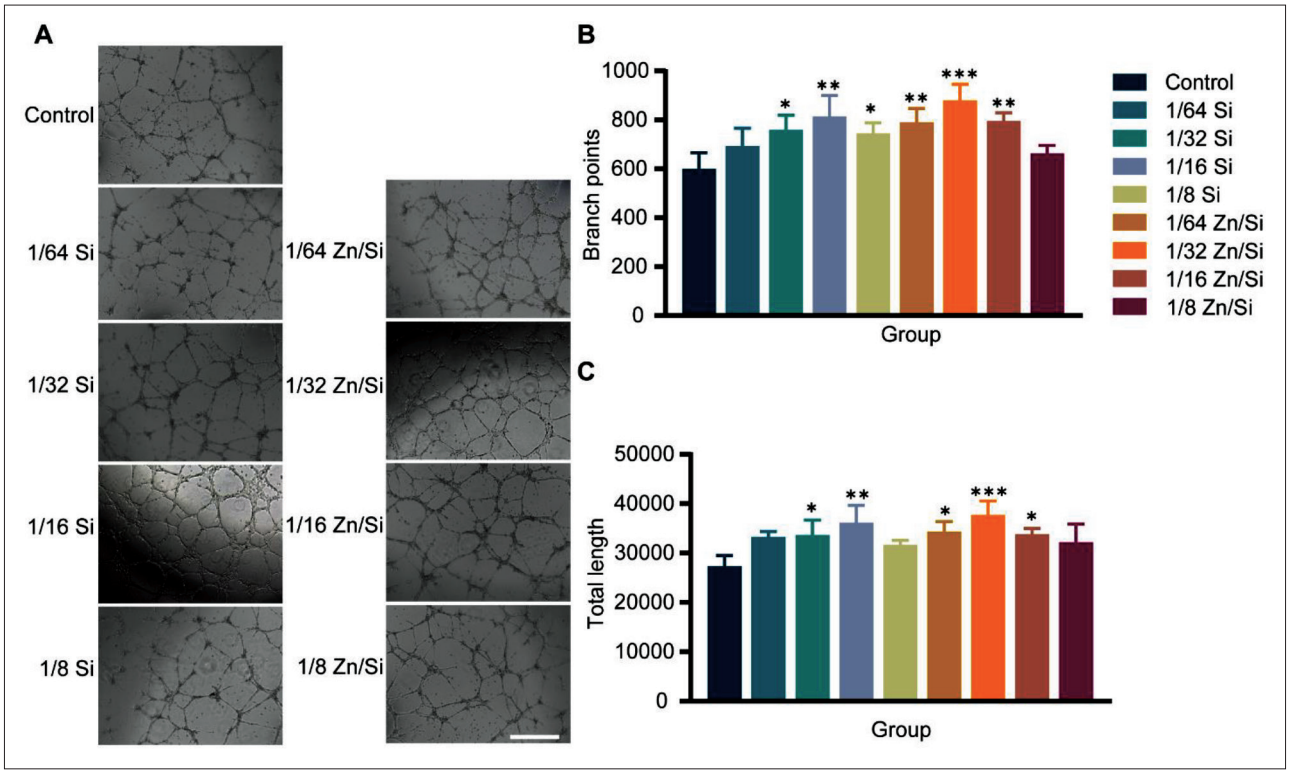

Figure 3. The proangiogenic effect of different concentrations of ions. (A) The typical images of tube formation of HUVECs with different treatments. (B, C) Quantitative analysis of tube formation ability. $^{*}P < 0.05$, $^{**}P < 0.01$, $^{***}P < 0.001$. N = 3 for each group. All the analyses were performed with one-way ANOVA. Scale bar = 200 μm.

pure GelMA hydrogel, GelMA-Zn/Si hydrogel showed no great changes in mechanical properties. Figure 4G presents typical compressive stress-strain curves of different hydrogels. The two curves almost coincide, and there is no difference in compressive modulus between the two hydrogels (Figure 4H).

The rheological properties of both hydrogels were investigated by frequency sweeping. Storage modulus (G′) and loss modulus (G″) of hydrogels were tested by time scanning. Figure 4I indicates that GelMA and GelMA-Zn/Si hydrogels have an identical point where G′ and G″ intersected with each other. The viscosities of both hydrogels have the same tendency with the increasing shear rate (Figure 4J). Frequency scanning reveals that the value of G′ is higher than that of G″ within an angular frequency range of 0.1–100 rad/s (Figure 4K). The ion release behavior of GelMA-Zn/Si hydrogel was evaluated by ICP. The results showed that the cumulative release of Zn and Si ions reached 0.363 μg/mL and 0.060 μg/mL, respectively, in 7 days (Figure 4L). For that, 1 mL GelMA-Zn/Si hydrogel was soaked in 9 mL PBS, the ion concentration was within biologically active concentration range after conversion. Taken together, our results suggest that GelMA-Zn/Si hydrogel has no changes in physicochemical properties compared to pure GelMA and is still suitable for treatment application.

3.5. Wound healing and regeneration of hair follicle in mice models

To determine whether ions promote *in situ* hair follicle regeneration *in vivo*, we introduced a mouse excisional model. As shown in Figure 5, there was no significant difference between the two groups on day 0 in the wound area. On day 7, the wound area of the control group greatly decreased, possibly due to the contraction of the wound without moisturizing, but the group showed more significant scar formation. At the time-point, we found that the GelMA-Zn/Si group had moister and smoother wounds without scar formation than other groups. Pure GelMA group also had relatively good wounds, which were better than hydrocolloid group. On day 14, all the treated groups almost achieved closure, while the control group still presented with detectable unhealed wounds. More interestingly, the GelMA-Zn/Si group had more significant hair follicle reappearance in the center of the wound and less scar formation based on gross observation, which indicates that GelMA-Zn/Si hydrogel can promote *in situ* hair follicle regeneration and reduce scar formation.

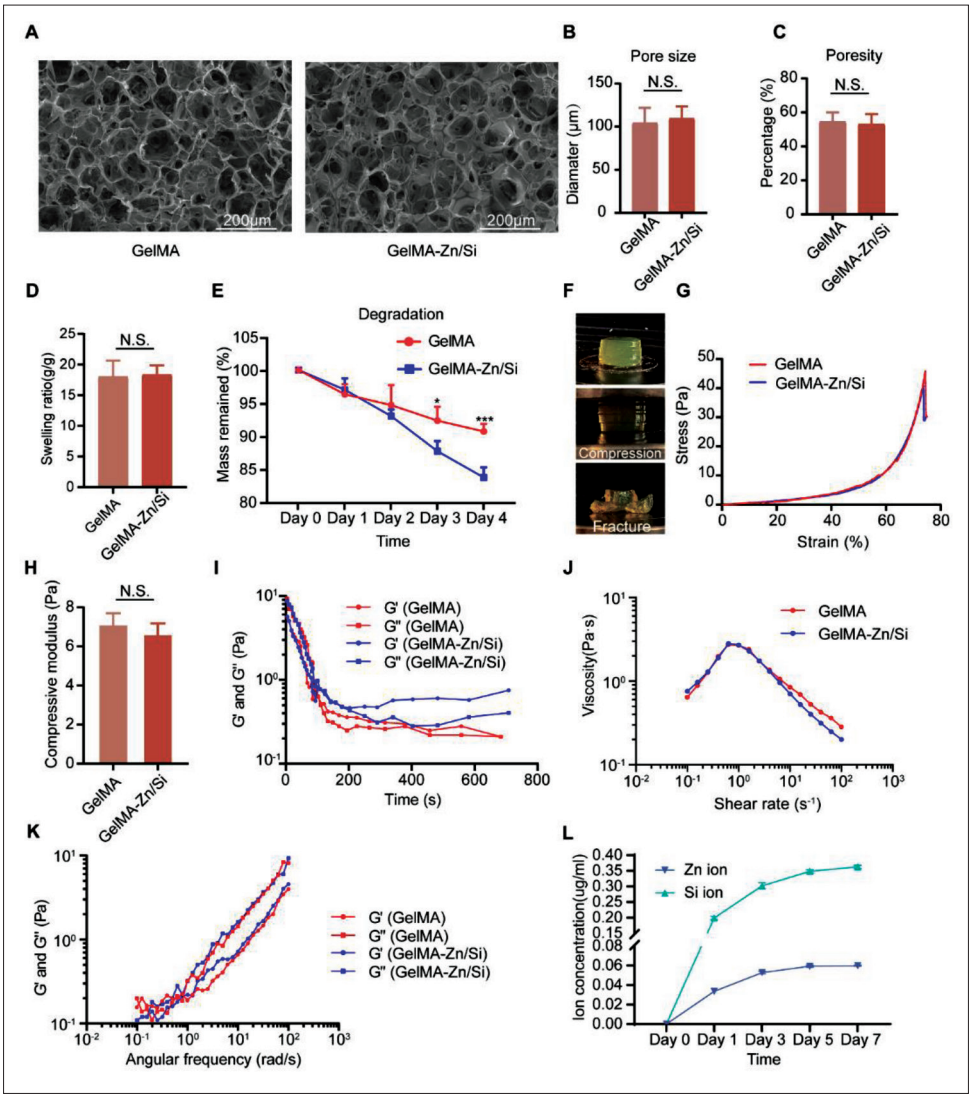

Figure 4. Characterization of hydrogels. (A) SEM images of GelMA and GelMA-Zn/Si hydrogels. (B, C) Comparison of the pore size and porosity of hydrogels. (D) Comparison of the swelling ratio of GelMA and GelMA-Zn/Si hydrogels. (E) Degradation of the GelMA and GelMA-Zn/Si hydrogels. (F) Typical images of the compression test process. (G) Typical compression stress–strain curves of the hydrogels. (H) The compressive modulus (15%–25% strain pressure) of different hydrogels. (I) G′ and G″ at an angular frequency of 1 Hz at 25°C. (J) Apparent viscosities of hydrogels under steady shear from 0.1 s^{-1} to 100 s^{-1} at 25°C. (K) G′ and G″ under steady angular frequency from 0.1 rad/s to 100 rad/s and an oscillatory strain of 5% at 25°C. (L) GelMA-Zn/Si hydrogel can release biologically active ions within 7 days. *$P < 0.05$, ***$P < 0.001$. N = 3 for each group. All the analyses in (B), (C), (D), and (H) were performed with an unpaired two-tailed *t*-test. The analyses in (E) were performed with two-way ANOVA.

3.6. Histological analysis

To further confirm hair follicle regeneration in GelMA-Zn/Si hydrogel group, H&E staining was performed on the samples. On the 14th day, GelMA-Zn/Si hydrogel group had the most hair follicles whereas the other groups nearly have no regeneration tendency (Figure 6A). Then, immunofluorescence staining was performed to observe HFSC marker K19[29]. After treatment with GelMA-Zn/Si hydrogel, the activation of HFSCs in the wound was determined. As compared with GelMA and hydrocolloid group, GelMA-Zn/Si hydrogel group had a larger number of $K19^+$ cells, indicating that hair follicle-related cells began to migrate and neogenic hair follicles started to grow (Figure 6B and C). In contrast, the control group had nearly no K19-positive staining. The results suggested that GelMA-Zn/Si hydrogel can activate HFSCs to promote hair follicle regeneration.

Vascularization of the wound areas is important to wound repair and tissue regeneration[30]. To observe the vessel regeneration, CD31 and α-SMA were stained in

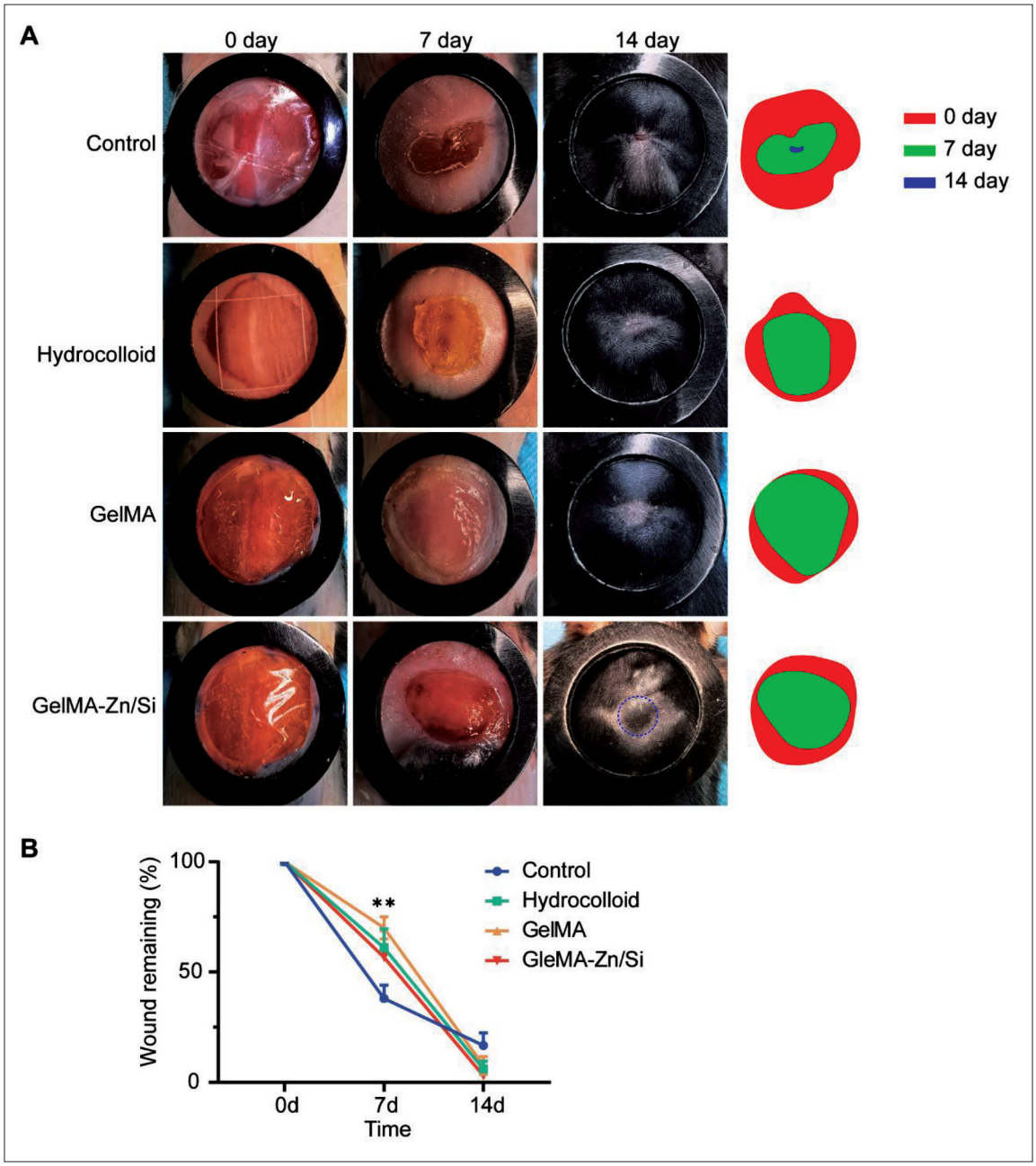

Figure 5. GelMA-Zn/Si hydrogel enhances *in situ* regeneration of hair follicle in mice excisional models. Gross appearance of the skin wounds. (A) Images were captured at 0, 7, and 14 days after operation. (B) Quantification of wound area. $^{**}P < 0.01$. The diameter of the rubber ring is 1 cm.

the wound tissue. The results showed that on the 14th day, GelMA-Zn/Si group had more positive staining in the wound areas, while less yellow staining was found in the other groups (Figure 6D). The quantitative analyses confirmed that GelMA-Zn/Si hydrogel group had the highest neovascularization, whereas GelMA and hydrocolloid groups only had a small amount of neogenic vessels (Figure 6E). These findings indicated that GelMA-Zn/Si hydrogel has stimulatory effects on angiogenesis.

3.7. Gene expression

To further investigate the effect of GelMA-Zn/Si hydrogel on hair follicle regeneration and angiogenesis, on the 14th day, the wound tissue was harvested and used for qRT-PCR (Figure 7). We determined the expression of hair follicle anagen markers, such as *Pdgfa* and *Pdgfb*[31]. The results indicated that GelMA-Zn/Si hydrogel group had the highest expression level, which means the hydrogel may stimulate hair follicle regeneration. The stem cell

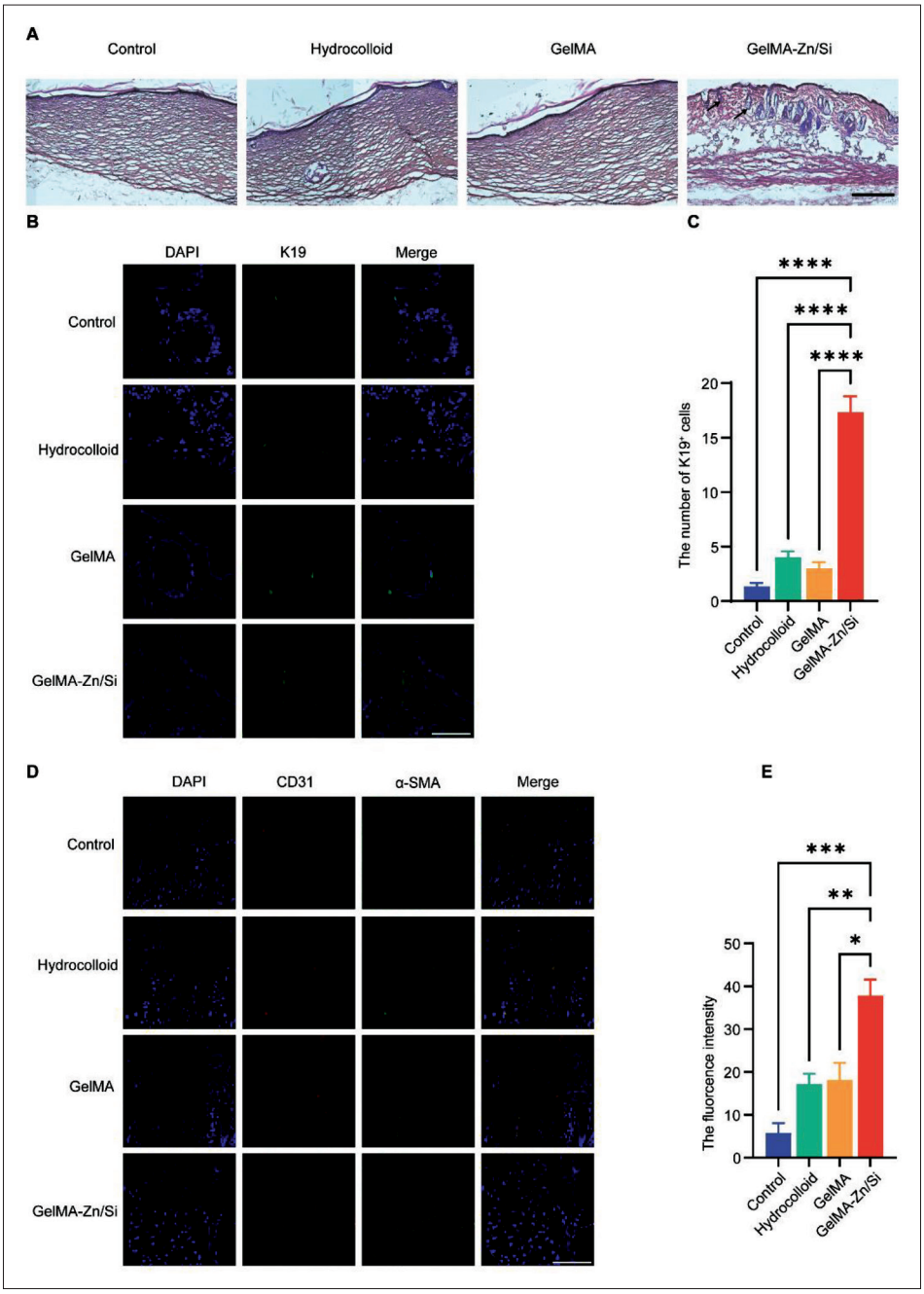

Figure 6. (A) Representative H&E-stained sections on the 14th day after treatment. Black arrows point to the neogenic hair follicles. (B) Representative immunofluorescence images on the 14th day after treatment show the presence of K19$^+$ cells. (C) Quantitative analysis of the number of K19$^+$ cells. (D) Representative immunofluorescence images on the 14th day after treatment show the presence of CD31/α-SMA$^+$ vessels. (E) Quantitative analysis of CD31/α-SMA$^+$ intensity (K19, green; CD31, red; α-SMA, green; DAPI, blue). N = 3 for each group. All the analyses were performed with one-way ANOVA. Scale bar = 200 μm (A); 100 μm (B, D).

markers, such as *Kgf* and *Egf*, were also detected in the study, and GelMA-Zn/Si hydrogel group had a stronger expression than others, suggesting that GelMA-Zn/Si hydrogel may promote the regeneration activity of the tissue[32]. Compared with other groups, GelMA-Zn/Si hydrogel greatly upregulated the expression of *Vegf*, which is related to angiogenesis. Insulin-like growth factor 1 is an important growth factor that stimulates endothelial cell migration and regulates neovascularization[33]. Similar to the results of *Vegf*, GelMA-Zn/Si hydrogel strongly upregulated the expression of *Igf1* and the data implies that GelMA-Zn/Si hydrogel may accelerate the formation of

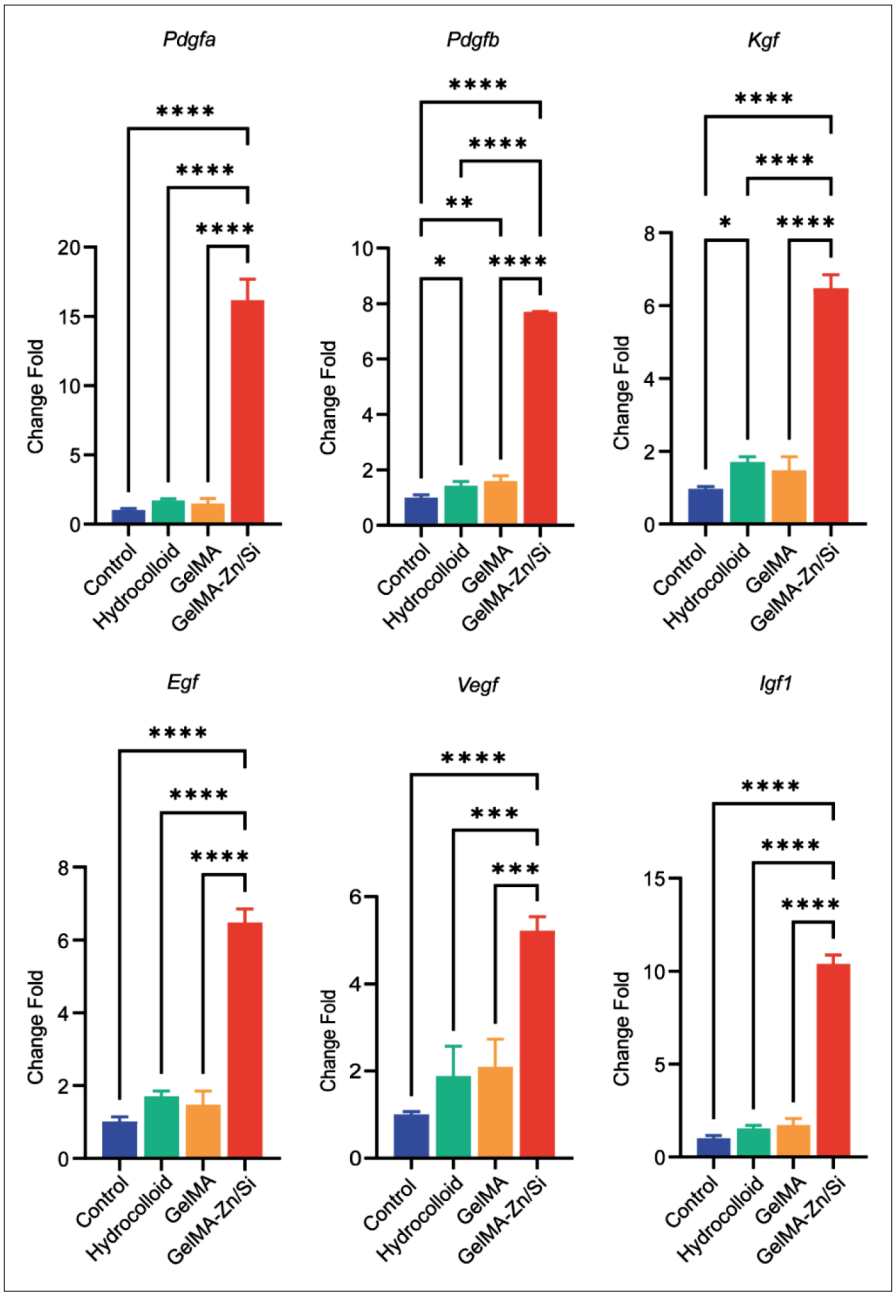

Figure 7. The relative gene expression of wound tissue on the 14th day after various treatments. *$P < 0.05$, **$P < 0.01$, ****$P < 0.0001$. N = 3 for each group. All the analyses were performed with one-way ANOVA.

neogenic vessels. More interestingly, GelMA group did not have significantly higher expression of most of the targeted genes, suggesting that the ions in the hydrogel may be the main effective factors in hair follicle regeneration and angiogenesis.

3.8. Perfusion recovery

Favorable blood perfusion contributes to wound healing and tissue regeneration[34]. Zn and Si ions can stimulate angiogenesis[9], and our results showed that GelMA-Zn/Si hydrogel group has the highest expression of angiogenesis-related genes. Therefore, laser Doppler perfusion measurement (LDPM) was employed to measure wound perfusion recovery in the scope to evaluate physiological and pharmacological changes of vascular function *in vivo*[35]. As shown in Figure 8, on 0 day, four groups had the same perfusion. On the 7th day, GelMA-Zn/Si hydrogel group presented with the richest blood flow signals, while

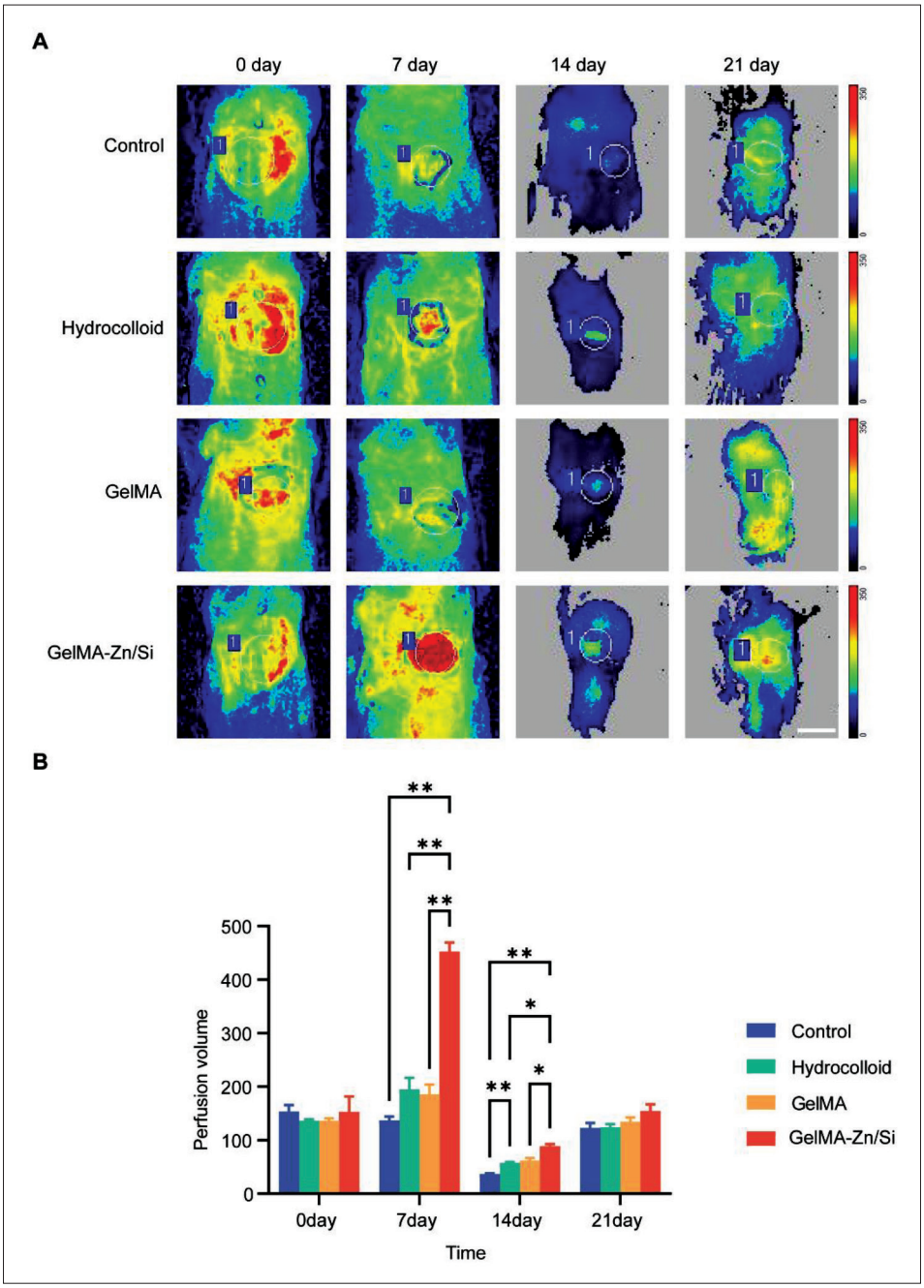

Figure 8. The blood flows at the wounds were measured by laser Doppler of animals. (A) Representative images of blood perfusion volume. The circle represents the position of the material. (B) Quantitative analysis of blood flow. N = 3 for each group. $^{*}P < 0.05$, $^{**}P < 0.01$. All the analyses were performed with two-way ANOVA. Scale bar = 1 cm.

the control group had the lowest intensity. Hydrocolloid and GelMA groups had the same perfusion level, which was lower than GelMA-Zn/Si group. In the follow-up study, four groups maintained low signal intensity for the coverage of neogenic epidermis, but GelMA-Zn/Si group always had the highest level. In short, the results showed that GelMA-Zn/Si hydrogel can improve wound perfusion after trauma, which is consistent with the results above.

4. Discussion

Most mammalian animals can achieve scar-free wound repair during their fetal development. However, the ability frequently disappears after birth[5]. Recent studies reported that the adult wound tissues still have the regenerative competence but the lack of regeneration signals contributes to the failure of tissue regeneration.

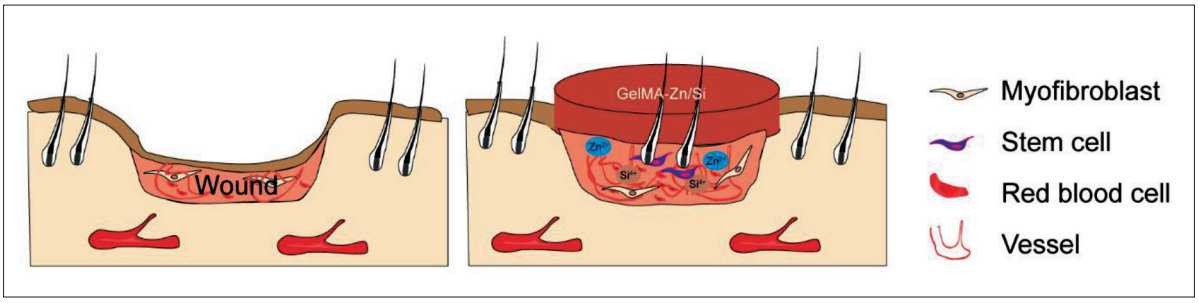

Figure 9. Proposed mechanism of GelMA-Zn/Si hydrogel promoting *in situ* regeneration of hair follicles in mouse excisional model.

Fibrosis and tissue regeneration are frequently believed to be opposing. Once the appropriate cues are modified, regeneration may be achieved after injury, rather than fibrotic repair[36,37]. Establishing developmental signals in dermis after trauma may be a practicable method to achieve regenerative repair[38,39]. Therefore, potential tools to revert skin cells to an "embryonic status" so as to achieve regeneration may be existing. In this study, we adopted GelMA loaded with bioactive ions and attempted to break the balance to regenerate hair follicles. As expected, the use of 3D-printed GelMA scaffold with mixed Zn/Si dual ions lead to an improvement in *in situ* hair follicle regeneration and wound healing.

Generally, both Zn and Si ions display good biocompatibility and stimulatory effect on fibroblasts, keratinocytes, and endothelial cells[9,40]. Further analyses indicate that 1/32 Zn/Si dual-ion solution is optimal because it can maximally improve fibroblasts wound healing and promote vessel tube formation. Zn ion solution alone cannot significantly influence the behavior of cells. Pure Si ion solution has the stimulatory effect but is slightly weaker than the mixture of two ions, implying that synergistic effects between the ions may be existing. Additionally, we investigated the effect of ions on hair follicle *in vitro* by employing DP cells, which are located at the base of hair follicle and play an important role in regeneration. The ions can promote migration and proliferation of DP cells, indicating the beneficial impact of ions on hair follicle *in vitro*. To overcome the limits of bioactive ions, in this work, the Zn/Si dual ions were incorporated into GelMA to prepare the GelMA-Zn/Si hydrogel and to match the demand of *in situ* regeneration.

To investigate the efficacy of this combination on stimulating hair follicle regeneration, we first verified that GelMA-Zn/Si hydrogel has no significant changes in physicochemical properties compared to pure GelMA hydrogel. After treatment, excisional wound healing in mice could recapitulate aspects of true tissue regeneration, i.e., the formation of new hair follicles, and presented with less scar formation. Intriguingly, in the gross observation, we noticed that GelMA-Zn/Si group had more hair in the wound center than other groups. Histological analysis also indicated that in GelMA-Zn/Si group, hair follicles started to grow in the center of the wound first and then spread to the margin. The phenomenon is named *in situ* hair follicle regeneration and has been considered the same as hair follicle development in the embryonic stage[5,41,42]. It has been reported that hair follicle neogenesis is regulated by microenvironment consisting of fibroblasts, stem cells and endothelial cells[43,44]. Our immunofluorescence results suggested that GelMA-Zn/Si hydrogel can activate HFSCs and angiogenesis to facilitate hair follicle regeneration. Apart from that, the expression of genes associated with angiogenesis and hair follicle development was significantly improved, which was not observed in the control group. Therefore, it is reasonable to assume that besides direct regulation through stem cells, ions may indirectly regulate hair follicle neogenesis via surrounding cells, such as endothelial cells. The speculation above was further confirmed by blood perfusion measurement, which showed that the mice treated with GelMA-Zn/Si hydrogel had more favorable blood perfusion. Good perfusion can provide sufficient nutrition and accelerate the transport of ions to the dermis to strengthen their biological effect, which may form a positive cycle in the end[45,46]. In addition, in this work, we employed *in situ* 3D bioprinting technology to print hydrogels to the wound. It has been reported that 3D bioprinting may provide the dressing with a tightly fitting surface and suitable topography and profoundly affect mechanotransduction, which may also contribute to the activation of hair follicle regeneration signaling pathways to some extent[47]. Therefore, we speculate that GelMA-Zn/Si hydrogel may provide signals to break the balance between scar formation and regenerative wound healing, and then, the repair process starts with cells reverted to "embryonic status" so as to achieve regenerative healing (Figure 9)[5].

Our study is the first to combine Zn/Si dual ions with GelMA to treat excisional wounds and achieve *in situ* regeneration of hair follicle. GelMA-Zn/Si hydrogel not

only has a stimulatory effect on stem cells, but also can promote angiogenesis and perfusion recovery, indicating that there are direct and indirect manners to regulate hair follicle regeneration. Although further work is required to illuminate the molecular mechanisms, integrating Zn/Si dual ions with GelMA hydrogel is an attractive option that opens new avenues for hair follicle regenerative skin repair.

5. Conclusion

In summary, we describe a feasible method to combine GelMA with Zn/Si dual ions to promote *in situ* hair follicle regeneration with the assistance of 3D bioprinting technology. Collectively, our *in vitro* and *in vivo* data underscore the capabilities of Zn/Si ions to impact the behavior of HFSCs and endothelial cells during hair follicle regeneration, which may directly or indirectly contribute to microenvironment manipulation of cell fate. The research also offers insights into promoting hair follicle regeneration.

Acknowledgments

The authors wish to acknowledge the assistance of Prof. Yuxia Zhao and Prof. Dong Qiu on materials characterization.

Funding

This study was supported by the Science Fund for National Defense Distinguished Young Scholars (2022-JCJQ-ZQ-016), Key basic research projects of the Foundation Strengthening Plan (2022-JCJQ-ZD-096-00), National Key Research and Development Program of China (2022YFA1104604), National Natural Science Foundation of China (32000969), and Key Support Program for Growth Factor Research (SZYZ-TR-03).

Conflict of interest

The authors declare no conflict of interest.

Author contributions

Conceptualization: Fanliang Zhang, Sha Huang, Bin Yao, Jiang Chang
Formal analysis: Fanliang Zhang, Xianlan Duan, Zhao Li
Funding acquisition: Sha Huang, Xiaobing Fu
Investigation: Fanliang Zhang, Zhaowenbin Zhang, Xianlan Duan, Yi Kong, Xing Huang
Methodology: Zhao Li, Wei Song, Bin Yao, Sha Huang, Yi Kong
Resources: Zhaowenbin Zhang, Wei Song, Xing Huang, Jiang Chang
Writing – original draft: Fanliang Zhang, Sha Huang
Writing – review & editing: Sha Huang, Xiaobing Fu

Ethics approval and consent to participate

Animals were maintained in a specific-pathogen-free facility of Chinese PLA General Hospital in accordance with the Guide for the Care and Use of Laboratory Animals. All animal experiments were approved by the Institutional Animal Care and Use Committee of Chinese PLA General Hospital (approval number SCXK(BJ)2017–0019).

Consent for publication

Not applicable.

Availability of data

The data that support the findings of this study are available from the corresponding authors upon reasonable request.

References

1. Gurtner GC, Werner S, Barrandon Y, *et al.*, 2008, Wound repair and regeneration. *Nature*, 453(7193):314–321.

   https://doi.org/10.1038/nature07039

2. Takeo M, Lee W, Ito M, 2015, Wound healing and skin regeneration. *CSH Perspect Med*, 5(1):a023267.

   https://doi.org/10.1101/cshperspect.a023267

3. Chuong CM, Randall VA, Widelitz RB, *et al.*, 2012, Physiological regeneration of skin appendages and implications for regenerative medicine. *Physiology*, 27(2):61–72.

   https://doi.org/10.1152/physiol.00028.2011

4. Ito M, Yang Z, Andl T, *et al.*, 2007, Wnt-dependent de novo hair follicle regeneration in adult mouse skin after wounding. *Nature*, 447(7142):316–320.

   https://doi.org/10.1038/nature05766

5. Lim CH, Sun Q, Ratti K, *et al.*, 2018, Hedgehog stimulates hair follicle neogenesis by creating inductive dermis during murine skin wound healing. *Nat Commun*, 9(1):4903.

   https://doi.org/10.1038/s41467-018-07142-9

6. Xing M, Jiang Y, Bi W, *et al.*, 2021, Strontium ions protect hearts against myocardial ischemia/reperfusion injury. *Sci Adv*, 7(3):eabe0726.

   https://doi.org/10.1126/sciadv.abe0726

7. Huang T, Zhang T, Jiang X, *et al.*, 2021, Iron oxide nanoparticles augment the intercellular mitochondrial transfer-mediated therapy. *Sci Adv*, 7(40):eabj0534.

   https://doi.org/10.1126/sciadv.abj0534

8. Zhang Z, Li W, Liu Y, *et al.*, 2021, Design of a biofluid-absorbing bioactive sandwich-structured Zn-Si bioceramic composite wound dressing for hair follicle regeneration and skin burn wound healing. *Bioact Mater*, 6(7):1910–1920.

   https://doi.org/10.1016/j.bioactmat.2020.12.006

9. Wang X, Gao L, Han Y, *et al.*, 2018, Silicon-enhanced adipogenesis and angiogenesis for vascularized adipose tissue engineering. *Adv Sci*, 5(11):1800776.

   https://doi.org/10.1002/advs.201800776

10. Li H, He J, Yu H, *et al.*, 2016, Bioglass promotes wound healing by affecting gap junction connexin 43 mediated endothelial cell behavior. *Biomaterials*, 84:64–75.

    https://doi.org/10.1016/j.biomaterials.2016.01.033

11. Sun Y, You Y, Jiang W, *et al.*, 2020, 3D bioprinting dual-factor releasing and gradient-structured constructs ready to implant for anisotropic cartilage regeneration. *Sci Adv*, 6(37):eaay1422.

    https://doi.org/10.1126/sciadv.aay1422

12. Kong L, Wu Z, Zhao H, *et al.*, 2018, Bioactive injectable hydrogels containing desferrioxamine and bioglass for diabetic wound healing. *ACS Appl Mater Interfaces*, 10(36):30103–30114.

    https://doi.org/10.1021/acsami.8b09191

13. Yue K, Santiago GT, Alvarez MM, *et al.*, 2015, Synthesis, properties, and biomedical applications of gelatin methacryloyl (GelMA) hydrogels. *Biomaterials*, 73:254–271.

    https://doi.org/10.1016/j.biomaterials.2015.08.045

14. Duan X, Yuan X, Yao B, *et al.*, 2022, The role of CTHRC1 in promotion of cutaneous wound healing. *Signal Transduct Target Ther*, 7(1):183.

    https://doi.org/10.1038/s41392-022-01008-9

15. Yuan X, Duan X, Enhejirigala, *et al.*, 2023, Reciprocal interaction between vascular niche and sweat gland promotes sweat gland regeneration. *Bioact Mater*, 21: 340–357.

    https://doi.org/10.1016/j.bioactmat.2022.08.021

16. Hu T, Cui X, Zhu M, *et al.*, 2020, 3D-printable supramolecular hydrogels with shear-thinning property: Fabricating strength tunable bioink via dual crosslinking. *Bioact Mater*, 5(4):808–818.

    https://doi.org/10.1016/j.bioactmat.2020.06.001

17. Zhou F, Hong Y, Liang R, *et al.*, 2020, Rapid printing of bio-inspired 3D tissue constructs for skin regeneration. *Biomaterials*, 258:120287.

    https://doi.org/10.1016/j.biomaterials.2020.120287

18. Chen M, Wu Y, Chen B, *et al.*, 2022, Fast, strong, and reversible adhesives with dynamic covalent bonds for potential use in wound dressing. *Proc Natl Acad Sci U S A*, 119(29):e2203074119.

    https://doi.org/10.1073/pnas.2203074119

19. Xia S, Weng T, Jin R, *et al.*, 2022, Curcumin-incorporated 3D bioprinting gelatin methacryloyl hydrogel reduces reactive oxygen species-induced adipose-derived stem cell apoptosis and improves implanting survival in diabetic wounds. *Burns Trauma*, 10:tkac001.

    https://doi.org/10.1093/burnst/tkac001

20. Galiano RD, Michaels J, Dobryansky M, *et al.*, 2004, Quantitative and reproducible murine model of excisional wound healing. *Wound Repair Regen*, 12(4):485–492.

    https://doi.org/10.1111/j.1067-1927.2004.12404.x

21. Yao B, Wang R, Wang Y, *et al.*, 2020, Biochemical and structural cues of 3D-printed matrix synergistically direct MSC differentiation for functional sweat gland regeneration. *Sci Adv*, 6(10):eaaz1094.

    https://doi.org/10.1126/sciadv.aaz1094

22. Gianni-Barrera R, Butschkau A, Uccelli A, *et al.*, 2018, PDGF-BB regulates splitting angiogenesis in skeletal muscle by limiting VEGF-induced endothelial proliferation. *Angiogenesis*, 21(4):883–900.

    https://doi.org/10.1007/s10456-018-9634-5

23. Yano K, Brown LF, Detmar M, 2001, Control of hair growth and follicle size by VEGF-mediated angiogenesis. *J Clin Invest*, 107(4):409–417.

    https://doi.org/10.1172/jci11317

24. Fredriksson I, Larsson M, Strömberg T, 2009, Measurement depth and volume in laser Doppler flowmetry. *Microvasc Res*, 78(1):4–13.

    https://doi.org/10.1016/j.mvr.2009.02.008

25. Abbasi S, Sinha S, Labit E, *et al.*, 2020, Distinct regulatory programs control the latent regenerative potential of dermal fibroblasts during wound healing. *Cell Stem Cell*, 27(3): 396–412.

    https://doi.org/10.1016/j.stem.2020.07.008

26. Brewer CM, Nelson BR, Wakenight P, *et al.*, 2021, Adaptations in Hippo-Yap signaling and myofibroblast fate underlie scar-free ear appendage wound healing in spiny mice. *Dev Cell*, 56(19):2722–2740.

    https://doi.org/10.1016/j.devcel.2021.09.008

27. Fernandes KJ, McKenzie IA, Mill P, *et al.*, 2004, A dermal niche for multipotent adult skin-derived precursor cells. *Nat Cell Biol*, 6(11):1082–1093.

    https://doi.org/10.1038/ncb1181

28. Grellier M, Bordenave L, Amedee J, 2009, Cell-to-cell communication between osteogenic and endothelial lineages: implications for tissue engineering. *Trends Biotechnol*, 27(10):562–571.

    https://doi.org/10.1016/j.tibtech.2009.07.001

29. Griffin DR, Archang MM, Kuan CH, *et al.*, 2020, Activating an adaptive immune response from a hydrogel scaffold imparts regenerative wound healing. *Nat Mater*, 20(4):560–569.

    https://doi.org/10.1038/s41563-020-00844-w

30. DiPietro LA, 2013, Angiogenesis and scar formation in healing wounds. *Curr Opin Rheumatol*, 25(1):87–91.

https://doi.org/10.1097/BOR.0b013e32835b13b6

31. Shabbir A, Cox A, Rodriguez-Menocal L, *et al.*, 2015, Mesenchymal stem cell exosomes induce proliferation and migration of normal and chronic wound fibroblasts, and enhance angiogenesis in vitro. *Stem Cells Dev*, 24(14):1635–1647.

https://doi.org/10.1089/scd.2014.0316

32. Rezza A, Sennett R, Tanguy M, *et al.*, 2015, PDGF signalling in the dermis and in dermal condensates is dispensable for hair follicle induction and formation. *Exp Dermatol*, 24(6):468–470.

https://doi.org/10.1111/exd.12672

33. Richardson GD, Bazzi H, Fantauzzo KA, *et al.*, 2009, KGF and EGF signalling block hair follicle induction and promote interfollicular epidermal fate in developing mouse skin. *Development*, 136(13):2153–2164.

https://doi.org/10.1242/dev.031427

34. Veith AP, Henderson K, Spencer A, *et al.*, 2019, Therapeutic strategies for enhancing angiogenesis in wound healing. *Adv Drug Deliv Rev*, 146:97–125.

https://doi.org/10.1016/j.addr.2018.09.010

35. Roche B, Vanden-Bossche A, Normand M, *et al.*, 2013, Validated laser Doppler protocol for measurement of mouse bone blood perfusion—Response to age or ovariectomy differs with genetic background. *Bone*, 55(2):418–426.

https://doi.org/10.1016/j.bone.2013.03.022

36. Choi YS, Zhang Y, Xu M, *et al.*, 2013, Distinct functions for Wnt/β-catenin in hair follicle stem cell proliferation and survival and interfollicular epidermal homeostasis. *Cell Stem Cell*, 13(6):720–733.

https://doi.org/10.1016/j.stem.2013.10.003

37. Plikus MV, Mayer JA, de la Cruz D, *et al.*, 2008, Cyclic dermal BMP signalling regulates stem cell activation during hair regeneration. *Nature*, 451(7176):340–344.

https://doi.org/10.1038/nature06457

38. Zhang L, Wang WH, Jin JY, *et al.*, 2019, Induction of hair follicle neogenesis with cultured mouse dermal papilla cells in de novo regenerated skin tissues. *J Tissue Eng Regen Med*, 13(9):1641–1650.

https://doi.org/10.1002/term.2918

39. Harn HI, Wang SP, Lai YC, *et al.*, 2021, Symmetry breaking of tissue mechanics in wound induced hair follicle regeneration of laboratory and spiny mice. *Nat Commun*, 12(1):2595.

https://doi.org/10.1038/s41467-021-22822-9

40. Zhai W, Lu H, Chen L, *et al.*, 2012, Silicate bioceramics induce angiogenesis during bone regeneration. *Acta Biomater*, 8(1):341–349.

https://doi.org/10.1016/j.actbio.2011.09.008

41. Xue Y, Lim CH, Plikus MV, *et al.*, 2022, Wound-induced hair neogenesis model. *J Invest Dermatol*, 142(10):2565–2569.

https://doi.org/10.1016/j.jid.2022.07.013

42. Gay D, Kwon O, Zhang Z, *et al.*, 2013, Fgf9 from dermal gammadelta T cells induces hair follicle neogenesis after wounding. *Nat Med*, 19(7):916–923.

https://doi.org/10.1038/nm.3181

43. Chueh SC, Lin SJ, Chen CC, *et al.*, 2013, Therapeutic strategy for hair regeneration: Hair cycle activation, niche environment modulation, wound-induced follicle neogenesis, and stem cell engineering. *Expert Opin Biol Ther*, 13(3):377–391.

https://doi.org/10.1517/14712598.2013.739601

44. Li KN, Tumbar T, 2021, Hair follicle stem cells as a skin-organizing signaling center during adult homeostasis. *Embo J*, 40(11):e107135.

https://doi.org/10.15252/embj.2020107135

45. Guerra A, Belinha J, Jorge RN, 2018, Modelling skin wound healing angiogenesis: A review. *J Theor Biol*, 459:1–17.

https://doi.org/10.1016/j.jtbi.2018.09.020

46. Bin BH, Bhin J, Takaishi M, *et al.*, 2017, Requirement of zinc transporter ZIP10 for epidermal development: Implication of the ZIP10-p63 axis in epithelial homeostasis. *Proc Natl Acad Sci U S A*, 114(46):12243–12248.

https://doi.org/10.1073/pnas.1710726114

47. Ma Y, Lin M, Huang G, *et al.*, 2018, 3D Spatiotemporal mechanical microenvironment: A hydrogel-based platform for guiding stem cell fate. *Adv Mater*, 30(49):e1705911.

https://doi.org/10.1002/adma.201705911